JACS
JOURNAL OF THE AMERICAN CHEMICAL SOCIETY
Article
pubs.acs.org/JACS

High-Pressure Synthesis and Characterization of $Li_2Ca_3[N_2]_3$—An Uncommon Metallic Diazenide with $[N_2]^{2-}$ Ions

Sebastian B. Schneider,[†] Markus Seibald,[†] Volker L. Deringer,[‡] Ralf P. Stoffel,[‡] Rainer Frankovsky,[†] Gina M. Friederichs,[†] Henryk Laqua,[∥] Viola Duppel,[⊥] Gunnar Jeschke,[∥] Richard Dronskowski,[‡,§] and Wolfgang Schnick*,[†]

[†]Department of Chemistry, Chair for Solid-State Chemistry, Ludwig Maximilian University, Butenandtstrasse 5-13, Munich 81377, Germany

[‡]Institute of Inorganic Chemistry, Chair of Solid-State and Quantum Chemistry, and [§]Jülich−Aachen Research Alliance (JARA-HPC), RWTH Aachen University, Landoltweg 1, Aachen 52056, Germany

[∥]Laboratory for Physical Chemistry, ETH Zürich, Wolfgang-Pauli-Strasse 10, Zürich 8093, Switzerland

[⊥]Max Planck Institute for Solid State Research Stuttgart, Heisenbergstrasse 1, Stuttgart 70569, Germany

Supporting Information

ABSTRACT: Dinitrogen (N_2) ligation is a common and well-characterized structural motif in bioinorganic synthesis. In solid-state chemistry, on the other hand, homonuclear dinitrogen entities as structural building units proved existence only very recently. High-pressure/high-temperature (HP/HT) syntheses have afforded a number of binary diazenides and pernitrides with $[N_2]^{2-}$ and $[N_2]^{4-}$ ions, respectively. Here, we report on the HP/HT synthesis of the first ternary diazenide. $Li_2Ca_3[N_2]_3$ (space group *Pmma*, no. 51, a = 4.7747(1), b = 13.9792(4), c = 8.0718(4) Å, Z = 4, wR_p = 0.08109) was synthesized by controlled thermal decomposition of a stoichiometric mixture of lithium azide and calcium azide in a multianvil device under a pressure of 9 GPa at 1023 K. Powder X-ray diffraction analysis reveals strongly elongated N−N bond lengths of d_{NN} = 1.34(2)−1.35(3) Å exceeding those of previously known, binary diazenides. In fact, the refined N−N distances in $Li_2Ca_3[N_2]_3$ would rather suggest the presence of $[N_2]^{3\cdot-}$ radical ions. Also, characteristic features of the N−N stretching vibration occur at lower wavenumbers (1260−1020 cm^{-1}) than in the binary phases, and these assignments are supported by first-principles phonon calculations. Ultimately, the true character of the N_2 entity in $Li_2Ca_3[N_2]_3$ is probed by a variety of complementary techniques, including electron diffraction, electron spin resonance spectroscopy (ESR), magnetic and electric conductivity measurements, as well as density-functional theory calculations (DFT). Unequivocally, the title compound is shown to be metallic containing diazenide $[N_2]^{2-}$ units according to the formula $(Li^+)_2(Ca^{2+})_3([N_2]^{2-})_3\cdot(e^-)_2$.

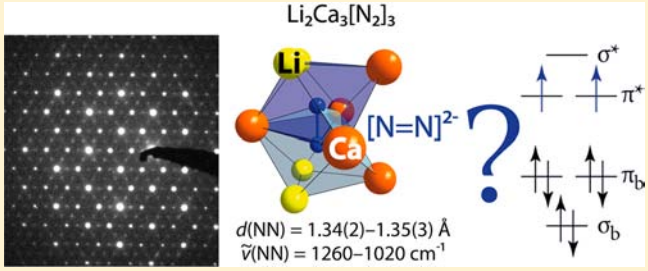

INTRODUCTION

Among the most important processes in modern chemistry is the conversion of dinitrogen molecules (N_2) into environmentally sustainable intermediates or products. This process is referred to as "nitrogen fixation". In industry, this process is named after its inventors Fritz Haber and Carl Bosch, the Haber-Bosch cycle,[1] which offers rapid access to synthetic fertilizers and has become essential for the nutrition of a large amount of the world population. In nature, this enormously expensive and complex industrial process is replaced by the enzyme nitrogenase, whose crystal structure has been determined only recently.[2] Nitrogenases can cleave the N≡N triple bond already at ambient conditions and transform it into ammonia, which however consumes huge amounts of energy (adenosine triphosphate, ATP).[3,4] Nitrogenase fixes atmospheric dinitrogen through an inimitable class of various metal clusters.[2,5−9] However, despite detailed knowledge of these structural motifs, a basic mechanism for the biological process still lacks evidence. Hence, the activation and conversion of free N_2 to ammonia including the characterization of a diversity of intermediates with bound dinitrogen is one of the major challenges in bioinorganic and organo-metallic chemistry, to finally unravel nature's mystery.[10]

Synthetic nitrogen fixation focuses on the binding, activation, and reduction of N_2 on mono-, di-, and polynuclear transition metal centers coordinated by capacious steric ligands. Mono- and dinuclear transition metal complexes have long been known to activate dinitrogen in various ways: they enable protonation, reduction, functionalization, and even N−N bond cleavage steps. Besides a handful of examples of transition metal complexes with trapped and activated N_2, up to date only two distinct classes of molybdenum- or tungsten-based model systems have emerged, involving a full set of well-defined

Received: August 26, 2013
Published: October 3, 2013

intermediates, such as diazenido, hydrazido, nitrido, imido, amido, or amine intermediates, on the way from N_2 to NH_3. These systems form the basis of the Chatt and the Schrock cycles.[11,12]

However, true mimicry of the multielectron reduction process still proves difficult because both cycles explain the sequence of reactions involved in biological dinitrogen reduction, on the one hand, but only a low yield catalytic reaction is observed in one of those systems, on the other hand.[11−23] The monometallic model systems of Chatt and Schrock cycles bind N_2 in an end-on manner and therefore lead to only weakly or moderately activated N_2-intermediates, which might be the crucial factor for the absence of a catalytic reaction. The binding of N_2 in a side-on manner is usually accessed by homonuclear bimetallic complexes. Common oxidation states for side-on bound N_2 when acting as a ligand are 0, −II, or −IV representing nonactivated dinitrogen(0), diazenido $[N_2]^{2-}$, or hydrazido $[N_2]^{4-}$ intermediates. This is not surprising as the dinitrogen ligand is reduced in multiples of two electrons, because each of the two metal atoms contributes either zero, one, or two electrons to nitrogen reduction. Odd-electron nitrogen oxidation states, instead, propose radical character and one-electron reduction mechanisms, but have not been observed in Chatt or Schrock cycles so far. However, this potential intermediacy of $[N_2]^{\cdot-}$ or $[N_2]^{3\cdot-}$ radical ions in metal complexes proved existence only very recently in dinuclear nickel, iron, and lanthanide complexes, respectively.[10,24−33] Thereby, $[N_2]^{\cdot-}$ were found to exhibit N−N bond lengths of about 1.13−1.18 Å and N−N stretching frequencies of 1740−1950 cm^{-1},[10,24−26,32,33] whereas the d_{NN} in $[N_2]^{3\cdot-}$ ions was found to be at 1.39−1.41 Å with shifted N−N stretching energies of below 1000 cm^{-1}.[27−33] To gain final evidence for the presence of such radical anions $[N_2]^{\cdot-}$ or $[N_2]^{3\cdot-}$, electron spin resonance spectroscopy (ESR) revealed clearly visible signals in accordance with simulated spectra indicative of unpaired electrons and supporting the radical formulation of dinitrogen ligation.[24,27,28]

Gauging "weakly" to "highly" activated systems is possible at the hand of N−N bond lengths and corresponding N−N stretching frequencies in spectroscopic studies of bound dinitrogen molecules or ions. For such purpose, reliable crystallographic and spectroscopic data for protonated reference compounds, such as diazene HN═NH and hydrazine N_2H_4, are required to facilitate the classification of even- and odd-electron nitrogen-oxidation states.

Surprisingly, given the importance of homonuclear dinitrogen anions in biological and organo-metallic chemistry, it was not before 2001 that such ions have been observed in solid-state chemistry for the first time.[34−39] Pioneering works by Kniep et al. introduced the hitherto unknown compounds Sr_4N_3 (≡ $Sr_8N_4[N_2]\cdot(e^-)_2$), SrN (≡ $Sr_8N_4[N_2]_2$), SrN_2, and BaN_2, which are the first so-called diazenides with ionic $[N_2]^{2-}$ units. The latter show characteristic N−N bond lengths (1.22 Å) and stretching frequencies (1307 cm^{-1} in SrN_2 and 1380 cm^{-1} in SrN), which may be compared to protonated diazene N_2H_2 (1.21−1.25 Å, 1400−1700 cm^{-1}).[34−45] Only 5 years later, high-pressure/high-temperature (HP/HT) experiments revealed the existence of noble metal compounds with MN_2 stoichiometry (M = Os, Ir, Pd, and Pt) exhibiting ultrahigh hardness and bulk moduli of about 250−350 GPa.[46−53] Theoretical investigations finally concluded the presence of tetravalent metals and $[N_2]^{4-}$ anions, with N−N bond lengths (about 1.40 Å) and stretching frequencies (700−1000 cm^{-1}) similar to those of hydrazine N_2H_4 (d_{NN} = 1.47 Å, $\tilde{\nu}_{NN}$ < 1000 cm^{-1}).[46−57] The latter anions are isoelectronic with peroxides $[O_2]^{2-}$, and so they were dubbed "pernitrides". In 2012, we were able to extend the compositional range of binary diazenides by subjecting ionic azides to HP/HT conditions in a multianvil device.[58,59] We succeeded in synthesizing SrN_2 and BaN_2, as well as the unprecedented (but theoretically predicted) CaN_2 and also Li_2N_2, the latter one representing the first alkali diazenide.[58−61] Crystallographic, spectroscopic, and theoretical investigations confirmed the presence of $[N_2]^{2-}$ anions in these crystal structures.[58,59] Only very recently, LaN_2 (≡ $La^{3+}[N_2]^{2-}\cdot e^-$) proved existence in shockwave experiments in accord with theoretical predictions.[54,62] Again, crystallographic studies showed the presence of diazenide anions with slightly elongated N−N bonds (1.30−1.32 Å), possibly due to the metallic character of the crystalline host.

In summary, the recent success in identifying diazenides and pernitrides in solid-state chemistry has fueled various theoretical and synthetic efforts to predict and characterize further compounds containing dinitrogen anions. However, despite the as-mentioned examples, no further representatives of diazenides, pernitrides, or even intermediate dinitrogen ions are known to date in ionic solids.

In this contribution, we present the successful synthesis and structural elucidation of $Li_2Ca_3[N_2]_3$, the first ternary compound with dinitrogen anions. Detailed crystallographic, spectroscopic, and theoretical studies at the respective state-of-the-art support the presence of solely $[N_2]^{2-}$ anions in the crystal structure. As we demonstrate, the title compound may be seen as the first ternary sub-diazenide with $(Li^+)_2(Ca^{2+})_3([N_2]^{2-})_3\cdot(e^-)_2$ formulation.

EXPERIMENTAL SECTION

Synthesis of $Li_2Ca_3[N_2]_3$. $Li_2Ca_3[N_2]_3$ was prepared under HP/HT conditions in a modified Walker-type module in combination with a 1000 t press (Voggenreiter, Mainleus, Germany). As pressure medium, Cr_2O_3 doped (5%) MgO-octahedra (Ceramic Substrates & Components, Isle of Wight, UK) with edge lengths of 18 mm (18/11 assembly) were employed. Eight tungsten carbide cubes (Hawedia, Marklkofen, Germany) with truncation edge lengths of 11 mm compressed the octahedron.

$Li_2Ca_3[N_2]_3$ can be synthesized from two different stoichiometric mixtures of lithium and calcium azides according to eqs 1 and 2. For a detailed description of the synthesis of both azides, see the Supporting Information.

$$2LiN_{3(s)} + 3Ca(N_3)_{2(s)} \rightarrow Li_2Ca_3[N_2]_{3(s)} + 9N_{2(g)} \quad (1)$$

$$2Li_{metal(s)} + 3Ca(N_3)_{2(s)} \rightarrow Li_2Ca_3[N_2]_{3(s)} + 6N_{2(g)} \quad (2)$$

The corresponding mixtures were carefully ground, filled into a cylindrical boron nitride crucible (Henze BNP GmbH, Kempten, Germany), and sealed with a fitting boron nitride plate. Details of the setup are described in the literature.[63−67] The assembly was compressed up to 9 GPa at room temperature within 213 min, then heated to 1023 K in 10 min, kept at this temperature for 20 min, and cooled to room temperature in 10 min again. Subsequently, the pressure was released over a period of 620 min. The recovered MgO-octahedron was broken apart in a glovebox (Unilab, MBraun, Garching; O_2 < 1 ppm, H_2O < 1 ppm), and the sample was carefully isolated from the surrounding boron nitride crucible. Besides a golden metallic powder of the title compound (see Figure S1 in the Supporting Information), which is very sensitive to moisture, small amounts of a red, but yet not identified, side-phase were obtained.

Powder X-ray Diffraction (PXRD). For powder X-ray diffraction experiments, ground $Li_2Ca_3[N_2]_3$ was loaded into tube capillaries (Hilgenberg, Malsfeld, Germany) with diameters of 0.2−0.3 mm in a

dx.doi.org/10.1021/ja408816t | J. Am. Chem. Soc. 2013, 135, 16668−16679

glovebox. Data were recorded with a STOE Stadi P powder diffractometer (STOE, Darmstadt, Germany) in Debye–Scherrer geometry using Ge(111) monochromated Cu and Mo $K_{\alpha 1}$ radiation (1.54056 and 0.7093 Å) with a step size of 0.01°. Data acquisition was done using the STOE software (WinXPOW). The indexing, integration, and extraction of the intensities as well as the structure solution and Rietveld refinement were performed with the TOPAS package (see Figure 1).[68]

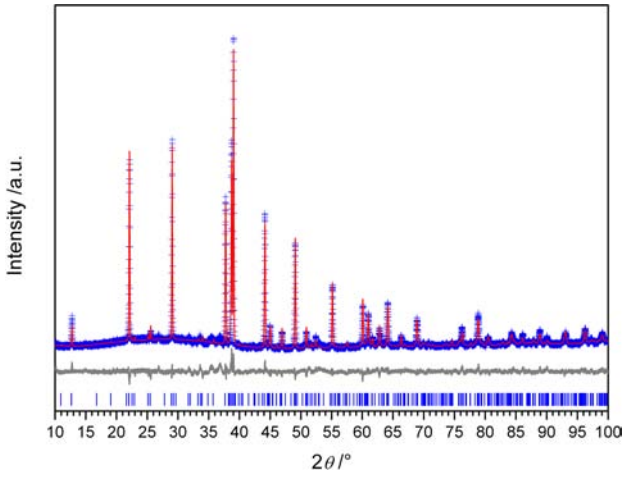

Figure 1. Observed (blue) and calculated (red) powder diffraction pattern (Cu $K_{\alpha 1}$ radiation, 1.54056 Å) and difference profile (gray) of the Rietveld refinement of $Li_2Ca_3[N_2]_3$. Peak positions are marked by vertical blue lines (bottom).

The reflection profiles were determined using the fundamental parameter approach[69] by convolution of appropriate source emission profiles with axial instrument contributions and crystalline microstructure effects. Preferred orientation of the crystallites was described with a spherical harmonic of fourth order. A search for potential higher symmetry obtained after structure solutions and Rietveld refinements was carried out using the program PLATON.[70] The relevant crystallographic data for the title compound as well as further details of the data collection are summarized in Tables 1 and S1 in the Supporting Information. Further information of the crystal structure may be obtained from the Fachinformationszentrum Karlsruhe, 76344 Eggenstein-Leopoldshafen, Germany (fax, (49) 7247-808-666; e-mail, crysdata@fiz-karlsruhe.de) on quoting the depository number CSD-426449.

Table 1. Refined Atomic Coordinates and Isotropic Displacement Factors of $Li_2Ca_3[N_2]_3$[a]

atom (Wyckoff)	x	y	z	U_{iso} (0.01 Å^2)[b]
Li1 (4*g*)	0	0.346(2)	0	0.033(9)
Li2 (4*h*)	0	0.847(3)	1/2	0.02(1)
Ca1 (2*e*)	1/4	0	0.697(1)	0.039(3)
Ca2 (2*f*)	1/4	1/2	0.195(2)	0.042(4)
Ca3 (4*k*)	1/4	0.1446(5)	0.164(1)	0.055(3)
Ca4 (4*k*)	1/4	0.6435(5)	0.651(1)	0.057(3)
N1 (4*k*)	1/4	0.177(1)	0.7043(9)	0.027(6)
N2 (4*k*)	1/4	0.6656(8)	0.2002(9)	0.048(9)
N3 (4*k*)	1/4	0.048(2)	0.410(4)	0.06(1)
N4 (4*k*)	1/4	0.548(1)	0.91(3)	0.027(7)
N5 (4*k*)	1/4	0.2860(8)	0.343(2)	0.026(5)
N6 (4*k*)	1/4	0.803(1)	0.867(1)	0.04(1)

[a]Space group *Pmma* (no. 51), a = 4.7747(1), b = 13.9792(4), c = 8.0718(4) Å, Z = 4. [b]$U_{iso} = B_{eq}/(8\cdot\pi^2)$.

High-temperature in situ X-ray powder diffraction data were collected with a STOE Stadi P powder diffractometer (Mo $K_{\alpha 1}$ radiation (0.7093 Å)) equipped with a computer-controlled STOE resistance graphite furnace. Enclosed in a silica glass capillary under argon, the samples were heated from room temperature to 700 K at a rate of 5 K/min in steps of 25 K (see Figure S2 in the Supporting Information). At each heating step (after holding the temperature for 1 min), a diffraction pattern was recorded with an IP-PSD in the range of $2° \leq 2\theta \leq 80°$. At about 610 K, the sample decomposed spontaneously.

Low-temperature in situ X-ray powder diffraction data were collected in intervals of 5 K using a Huber G670 Guinier imaging plate diffractometer (Co $K_{\alpha 1}$ radiation (1.7890 Å)) equipped with a closed cycle He-cryostat. The samples were cooled from room temperature to 10 K in 5 K/min. At each cooling step (after holding the temperature for 1 min), a diffraction pattern was recorded in the range of $10° \leq 2\theta \leq 80°$. No phase transition was observed.

Transmission Electron Microscopy (TEM). All manipulations for the preparation and transfer of the sample were carried out under argon atmosphere. Data were recorded with a Philips CM30/ST (LaB_6 cathode) at 300 kV. Selected area electron diffraction (SAED) as well as precession electron diffraction patterns (PED) were collected with a GATAN slow-scan CCD camera. Simulations of diffraction patterns were calculated with the EMS program package.[71] Elemental analysis by EDX was performed with a Si/Li detector (Thermo Fischer, NSS). Tilt series of diffraction patterns were obtained using a double tilt sample holder with a maximum tilt angle of ±25°.

Computational Details. Periodic density-functional theory (DFT) computations in the generalized gradient approximation of Perdew, Burke, and Ernzerhof (PBE)[72] were done using the projector augmented-wave (PAW)[73] method as implemented in the Vienna ab initio Simulation Package (VASP).[74] The cutoff energy for the plane-wave expansion was set to 500 eV, and the Brillouin zone was sampled on a dense Monkhorst-Pack mesh of reciprocal-space points.[75] Electronic wave functions (crystal structures) were optimized until the energy difference between two iterative steps fell below 10^{-8} eV/cell (10^{-6} eV/cell), respectively.

Chemical-bonding analyses were performed by computing the crystal orbital Hamilton population (COHP),[76] which allows one to identify bonding and antibonding contributions to the electronic band structure by weighting the off-site projected DOS with the corresponding Hamiltonian matrix elements (hence, negative COHP values denote stabilizing interactions). These computations were done for the previously optimized structures using the TB-LMTO-ASA program,[77] version 4.7, as in our previous studies of diazenides.[54,58−60] In this case, the local von Barth-Hedin exchange-correlation functional[78] had to be employed to ensure convergence.

Vibrational properties such as phonon densities of states were calculated by the ab initio force-constant method[79] as implemented in the FROPHO code[80] based on forces obtained from VASP.

Electron Spin Resonance Spectroscopy (ESR). ESR measurements were carried out on powdered samples covering a temperature range of 10−525 K. For that, the sample was filled into a quartz Mark tube capillary (diameter: 0.3 mm) and sealed under inert conditions. Low-temperature (ambient temperature to 10 K) continuous-wave (CW) ESR measurements at X-band frequencies were performed on three spectrometers: (a) on a Bruker Elexsys 500 CW ESR spectrometer equipped with a Bruker ER 4122 SHQ resonator with or without an Oxford Helium flow cryostat, (b) on a Bruker Elexsys 580 X-band CW/pulse ESR spectrometer equipped with a Bruker dielectric ENDOR resonator and an Oxford Helium flow cryostat, and (c) on a Magnetech MS 400 miniscope spectrometer equipped with a nitrogen flow cryostat. High-temperature (ambient temperature to 525 K) measurements were carried out on spectrometer (a). All measurements were properly calibrated and referenced to standards as detailed in the Supporting Information.

Fourier Transform Infrared Spectroscopy (FTIR). Fourier transform infrared spectroscopy measurements were carried out on a Bruker FTIR-IS66 V-S spectrometer. Spectra of the samples were

recorded at ambient conditions between 400 and 4000 cm^{-1} after the samples were diluted in dried KBr pellets under inert conditions.

Magnetic and Electric Conductivity Measurements. The magnetic measurements were performed on a Quantum Design MPMS XL5 SQUID magnetometer. Electric resistivity and conductivity were determined from a cold pressed (10 kN) pellet of nonsintered $Li_2Ca_3[N_2]_3$ (diameter 4.0 mm, thickness 1.28 mm) using the four-probe method. For the measurement, three batches of previously synthesized $Li_2Ca_3[N_2]_3$ had to be combined due to the small sample amount obtained upon one HP/HT experiment. In addition, each product of synthesis was analyzed separately by means of powder X-ray diffraction to rely on a successful synthesis. The pellet was contacted with four equidistant probes using silver conducting paint. As the compound is very sensitive to moisture, all preparations had to be done in a glovebox. A current of 5.0 mA was applied and the potential difference was measured as a function of temperature (3.5–300 K) yielding the resistivity. No superconductivity was observed.

RESULTS AND DISCUSSION

Unit-Cell Metrics. The unit-cell metrics was analyzed on the basis of powder X-ray diffraction (PXRD) and transmission electron microscopy (TEM) data. The indexing of PXRD patterns suggested a unit cell with hexagonal metrics (a = 8.06, c = 4.76 Å). From systematic absences, as well as from the integration and extraction of the intensities, a first structural model in space group $P6_3/mcm$ (no. 193) was derived (see Figures S4–S6 in the Supporting Information). However, SAEDs with the hexagonal $[001]_{hex}$ zone axis of all investigated crystallites significantly differed from simulated ones (see Figure 2). Hereby, the experimental diffraction patterns of

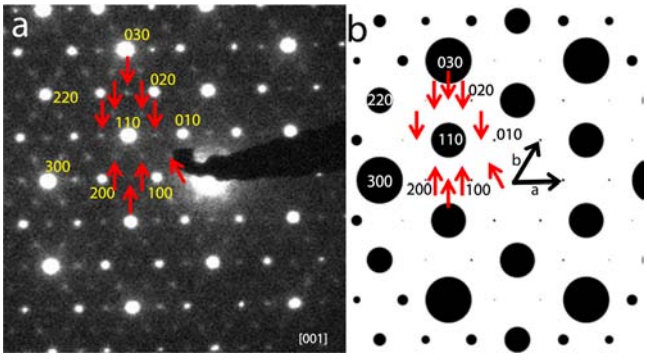

Figure 2. Experimental (a) and simulated (b, hexagonal model with a = 8.06, c = 4.76 Å) SAED pattern of $[001]_{hex}$ zone axis of hexagonal "$LiCaN_2$". In the experimental SAED pattern, between each indexed spot, there are further residual spots (red arrows). According to the simulated SAED pattern, these additional reflections suggest a doubling of the unit cell according to $a' = 2a$ and $b' = 2b$.

$[001]_{hex}$ zone axes contain additional reflections that suggest a doubling of the unit cell axes a and b. Although simulated diffraction patterns of $[001]_{hex}$ zone axes of an isomorphic subgroup with $a' = 2a$ and $b' = 2b$ ($P6_3/mcm$, no. 193) would result in the experimentally observed diffraction profile, the simple doubling of the lattice parameters does not fit other zone axes due to a simulated, doubled spot density that is absent in the experimental diffraction patterns. Therefore, a simple doubling of the lattice parameters does not suffice to reconcile experimental and simulated diffraction patterns.

As it was not possible to describe all diffraction patterns with the obtained hexagonal model, reduction of symmetry was done referring to group-subgroup relations. A first translationsgleich reduction in symmetry of index 3 (structure model in hexagonal space group $P6_3/mcm$, no. 193) results in the orthorhombic space group $Cmcm$ (no. 63) with a = 13.96, b = 8.06, and c = 4.76 Å. The C-centering, however, still results in an extinction of reflections with $h + k = 2n + 1$, and hence the simulated diffraction pattern of the [001] zone axis in $Cmcm$ is similar to the one of the hexagonal model. Thus, the C-centering has to be omitted and the symmetry further reduced in a second step. This klassengleich symmetry reduction of index 2 into space group $Pmma$ (no. 51) finally results in an adequate model. The simulated diffraction pattern of the resulting $[100]_{orth}$ zone axis (former [001] zone axes in $P6_3/mcm$ and $Cmcm$) matches the experimental reflection profile for the latter model by additional stepwise tilting by 120° around the origin of $[100]_{orth}$ zone axes quite well (see Figure 3) and indicates a $[100]_{orth}$ (=$[001]_{hex}$) stacked 3-fold twin.

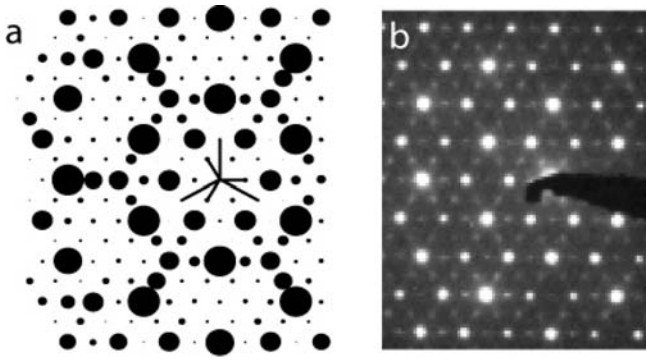

Figure 3. (a) Simulated SAED pattern of 3-fold twin by rotation in orthorhombic space group $Pmma$ (no. 51) obtained after stepwise tilting the simulated $[100]_{orth}$ pattern by 120° around the origin. (b) Experimental SAED pattern of former hexagonal $[001]_{hex}$ zone axis matching the diffraction profile of the 3-fold twin.

The latter, orthorhombic unit-cell metrics is supported by comparison of experimental SAED patterns to simulated ones; zone axes and lattice parameters have been obtained by transformations of the former hexagonal model (see the Supporting Information).

In addition, the theoretical positions of reflections of the as-obtained model are consistent with the experimentally observed positions in the corresponding PXRD patterns, resulting in Pawley-fitted parameters of a = 4.7747(1), b = 13.9792(4), and c = 8.0718(4) Å in space group $Pmma$ (no. 51). Note that as-investigated hexagonal and orthorhombic models mentioned in this section exhibit stoichiometric compositions of "$LiCaN_2$" diverging from elemental analysis which suggested lithium-deficiency (see the following sections).

Theoretical Considerations on the Hexagonal Model. The complex nature of the problem at hand called for a complementary quantum-theoretical analysis in search of the structure, and the first computations were performed for the initially assigned, hexagonal model with "$LiCaN_2$" composition ($P6_3/mcm$, see Supporting Information Figure S4). Surprisingly, at first sight, this structure showed pronounced instability during relaxation: the Hellmann-Feynman forces computed at temperature zero were enough to totally destroy the Li–Ca coordination environment. Moreover, phonon computations characterize this structure as dynamically unstable, proven by the presence of several imaginary eigenmodes (see Figure 4a). To improve this structural model, we applied a multistep

dx.doi.org/10.1021/ja408816t | J. Am. Chem. Soc. 2013, 135, 16668–16679

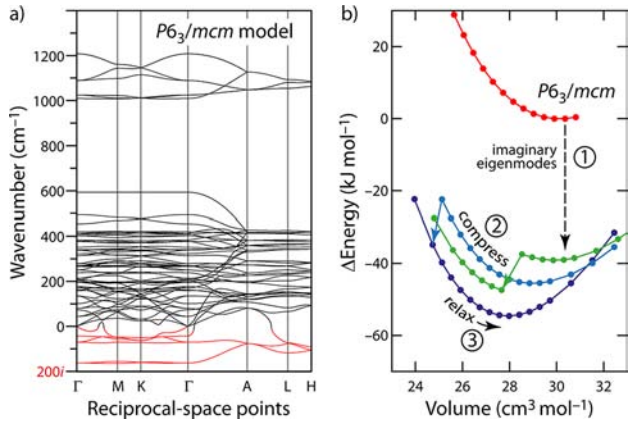

Figure 4. (a) Phonon band structure computed for the hexagonal $P6_3/mcm$ model exhibiting "$LiCaN_2$" stoichiometry. Several imaginary eigenvalues (highlighted in red), seemingly extending throughout the entire Brillouin zone, are visible. (b) Energy-volume plots for the different structural models of "$LiCaN_2$", with arrows describing how one is obtained from the other. Lines connecting data points are only guides to the eye. See text for discussion.

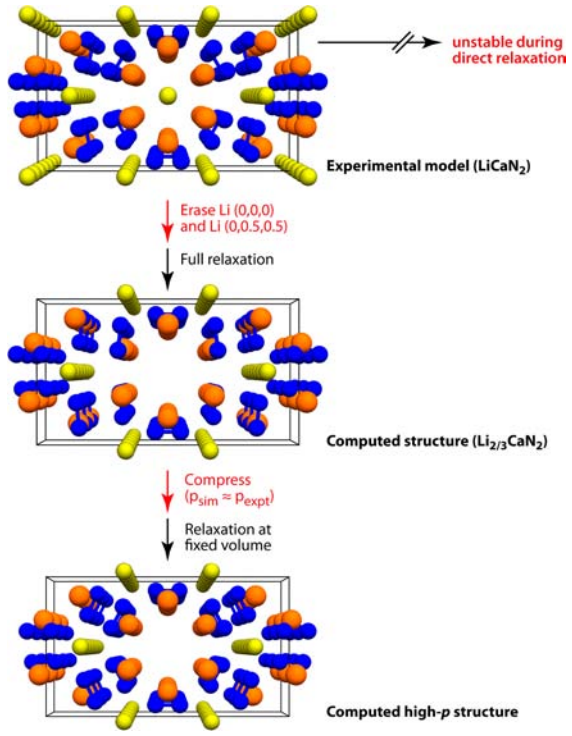

Figure 5. Schematic drawing of the route from the initial experimental, orthorhombic "$LiCaN_2$" model to the final, Li-deficient model with $Li_2Ca_3[N_2]_3$ stoichiometry, both of which exhibit space group *Pmma* (no. 51). Cell sizes are not to scale; Li yellow, Ca orange, N blue.

procedure that has been described in more detail recently.[81] First, we applied eigenvectors of the imaginary modes at the Γ point followed by structural optimization, for which the $E(V)$ plot is shown in Figure 4b. This process, labeled (1) in Figure 4b for two distinct eigenmodes, leads to the new $E(V)$ curves shown in green and light blue, respectively. This structural change is accompanied by an energy gain of over 30 kJ/mol, quite impressively. For both of these structures, subsequent energy-volume scans were performed (labeled (2)). Upon compressing the simulated cells, both still showed an inherent instability upon decreasing the unit-cell volume below ~28 cm^3 mol^{-1} (green dots) or ~25 cm^3 mol^{-1}, respectively. The most favorable structure, finally, was obtained upon relaxation (labeled (3); dark blue line in Figure 4b) and led to an energy gain of ~55 kJ/mol as compared to the initial $P6_3/mcm$ guess.

The new theoretical structure with "$LiCaN_2$" composition was found in space group *Pmma* (no. 51). It must be noted, however, that the resulting space group equals that of the TEM model (see previous section) only by coincidence, and the reason is as follows. Despite the large energetic stabilization of ~55 kJ mol^{-1} gained during the optimization procedure that started from the initial model ($P6_3/mcm$, Figure 4b), a simulated diffraction pattern for the optimized "$LiCaN_2$" model could not be reconciled with the experimental diffractogram. In particular, the computational result so far did not correspond to the revised unit-cell metrics but to those of the initial model, which had been falsified in the sequel. Consequently, what was initially believed to be the "correct" answer from theory (Figure 4b, dark blue curve) had to be discarded in the light of experiment.

On the other hand, the revised structural model derived from TEM (sketched in Figure 5, top) again proved unstable during quantum-chemical relaxation. This led us to conclude that the results of the elemental analysis (see the Supporting Information) had to be recalled as the compound obtained from HP/HT experiments might differ in stoichiometry as compared to the originally proposed sum formula of $LiCaN_2$.

Improving the Structural Model. The elemental analysis, albeit with some uncertainty, suggested a Li deficiency with a atomic ratio Li:Ca ≈ 0.8:1 in the title compound, whereas a Ca:N ratio of ~1:2 had been observed. Also, the exclusively Ca-coordinated Li positions in the *Pmma* structure model (2*a* and 2*d*) were the ones that experienced the most pronounced structural change/instability in the theoretical computations. Hence, it became obvious that the structural model with Li:Ca = 1 did not suffice because it did not lead to an agreement of experiment and theory.

Indeed, upon removing the Li atoms in question, the stoichiometric composition was changed to $Li_2Ca_3[N_2]_3$, and we again carried out structural optimizations (see Tables S3 and S4 in the Supporting Information), starting from the TEM-based experimental, orthorhombic "$LiCaN_2$" model in space group *Pmma* (see Figure 5) but with Li deficiency at 2*a* and 2*d* sites.

In the absence of external pressure, the structure seemed to be unstable again as indicated by the presence of imaginary phonon modes (albeit less strongly pronounced than in the $P6_3/mcm$ model characterized in Figure 4a). Nonetheless, by decreasing the simulation cell volume, the proposed structure could be stabilized. The imaginary modes disappeared entirely once the simulated pressure increased to ~13 GPa and above (see Figure 6), which is close to synthesis conditions (9 GPa). The imaginary eigenmodes at zero pressure might propose further instability of the crystal structure at ambient conditions; however, a collapse of the crystal structure at these conditions seems to be kinetically hindered as $Li_2Ca_3[N_2]_3$ could be analyzed experimentally even after releasing high pressure.

Note that the spot density in simulated diffraction patterns of $Li_2Ca_3[N_2]_3$ (data not shown) is equal to orthorhombic "$LiCaN_2$" in space group *Pmma* (no. 51, TEM-based model). It is only the intensity of the spots that slightly varies due to the lithium depletion of Wyckoff positions 2*a* and 2*d* in "$LiCaN_2$" resulting in the composition $Li_2Ca_3[N_2]_3$. Thus, the simulated

dx.doi.org/10.1021/ja408816t | J. Am. Chem. Soc. 2013, 135, 16668−16679

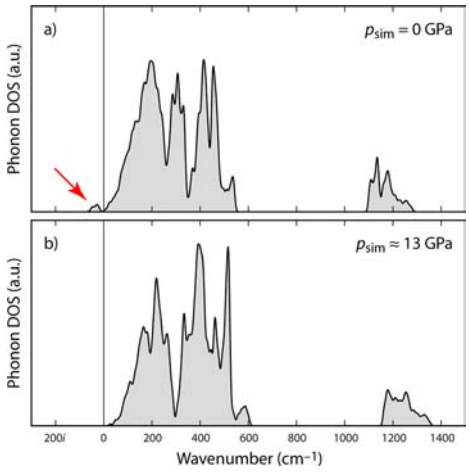

Figure 6. Computed phonon DOS for the final structural model with $Li_2Ca_3[N_2]_3$ stoichiometry without external pressure (a) and at a simulated pressure of approximately 13 GPa (b). In the upper panel, a small number of imaginary eigenmodes are visible as indicated by a red arrow. In the lower panel, these imaginary modes have disappeared, and the structural model proves dynamically stable.

diffraction patterns are also in good agreement with the final crystal structure.

Description of the Crystal Structure. $Li_2Ca_3[N_2]_3$ shows a close structural relationship to hexagonal Mn_5Si_3-type structures ($P6_3/mcm$, no. 193), better known as Nowotny phases.[82−84]

$Li_2Ca_3[N_2]_3$ contains four pairs of crystallographically independent nitrogen dumbbells exhibiting N−N bond lengths of d_{NN} = 1.337(17)−1.353(32) Å (see Figure 7 and Table 2).

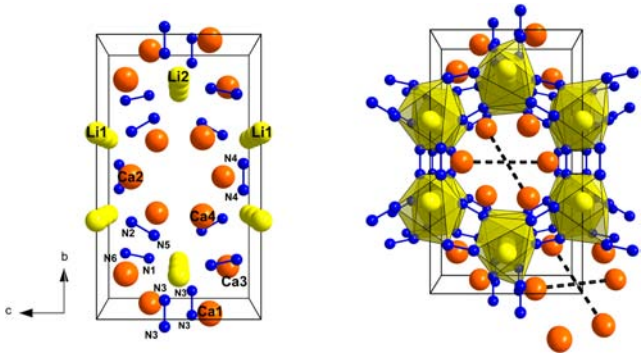

Figure 7. Unit cell of $Li_2Ca_3[N_2]_3$ viewed along [100] as resulting from the final refinement. Polyhedra around Li atoms are marked in yellow; Li yellow, Ca orange, N blue. Dashed lines in the right figure represent Ca−Ca distances in the center of the unit cell with $d_{Ca1-Ca1}$ = 5.45(1), $d_{Ca2-Ca2}$ = 5.47(2), $d_{Ca3-Ca3}$ = 5. 39(1), and $d_{Ca4-Ca4}$ = 5.267(9) Å, respectively. For further information, see Table S6 in the Supporting Information.

These N−N distances are intermediate to those in experimentally reported diazenides MN_2 (M = Ca, Sr, Ba), Li_2N_2 and LaN_2 having distances of about 1.20−1.32 Å,[58,59,62] and to pernitride $[N_2]^{4-}$ ions with N−N bond lengths of about 1.40 Å.[46−54] For $Li_2Ca_3[N_2]_3$, this suggests a $[N_2]^{3\cdot-}$ formulation, which would correspond to a radical character of the dinitrogen anion. In more detail, as-obtained N−N distances are in good agreement with corresponding characteristics of $[N_2]^{3-}$ ligation observed in already mentioned bimetallic lanthanide complexes (d_{NN} = 1.39−1.41 Å).[10,27−31]

Table 2. Experimental and Computationally Optimized N−N Bond Lengths (in angstroms) of Nitrogen Dumbbells in $Li_2Ca_3[N_2]_3$, Together with π^* Orbital Fillings (See Text)

N_x−N_y[a]	1−6	2−5	3−3	4−4	average
exp.	1.342(14)	1.337(17)	1.353(32)	1.348(26)	
calcd at 0 GPa	1.308	1.308	1.313	1.313	
π^* filling	55%	59%	59%	56%	57%
calcd at 16 GPa	1.293	1.293	1.291	1.289	
π^* filling	55%	51%	59%	46%	53%

[a]The pairing of six crystallographically independent nitrogen sites (all Wyckoff site 4*k*), thereby referring to Table 1, results in four crystallographically independent N_2 entities.

However, recent theoretical calculations considering hypothetical TiN_2 also support diazenide $[N_2]^{2-}$ units with N−N bond lengths up to even 1.46 Å.[85]

To elucidate the electronic character of the dinitrogen anion, we targeted chemical bonding analysis by means of the crystal orbital Hamiltonian population (COHP) method, as done previously for different diazenide/pernitride compounds.[54,58−60]

Figure 8 shows the well-known electronic "fingerprint" of the dinitrogen entity in the region close to the Fermi level ε_F.[54] In

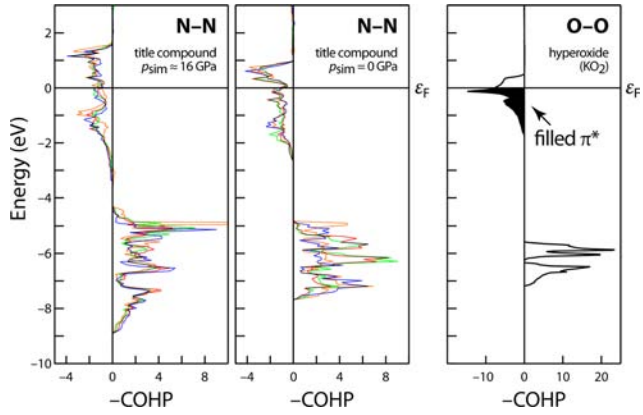

Figure 8. Left and middle: COHP analysis for the 4 $[N_2]$ entities in $Li_2Ca_3[N_2]_3$ depicted in different arbitrarily chosen colors, computed under a pressure of 16 GPa (left) and for the fully relaxed structure at zero pressure (middle), respectively. For the definition of π^* filling, see the text. Right: Same but for the $[O_2]$ entity in potassium hyperoxide KO_2.

agreement with Scheme 1, a set of π bonding and π^* antibonding bands may be discerned. The four dinitrogen dumbbells, despite overall similarities, have a unique bonding fingerprint each (shown in different colors), which is in accord with the experimental observation of several N−N stretching modes in the vibrational spectrum. For a more quantitative analysis, we calculate the "filling" of the π^* orbitals as reflected in the integrated COHPs. (We are aware of difficulties in integrating over an unoccupied area of the band structure; relative comparison is however well permitted.) We derive the filling as

$$\left(\int_{\varepsilon_-}^{\varepsilon_F} \mathrm{COHP}(E)\,\mathrm{d}E\right)/\left(\int_{\varepsilon_-}^{\varepsilon_+} \mathrm{COHP}(E)\,\mathrm{d}E\right)$$

dx.doi.org/10.1021/ja408816t | J. Am. Chem. Soc. 2013, 135, 16668−16679

Scheme 1. Schematic Molecular-Orbital Diagrams (Not Drawn to Scale) for the Species Discussed[a]

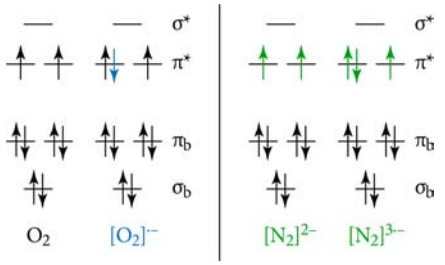

[a]Electrons in excess of the neutral diatomic ground state are indicated in color.

where ε_- denotes a suitably chosen lower energy limit (in Figure 8, 4 eV below the Fermi level) and ε_+ is the upper one (2 eV above ε_F). The resulting values of the π^* filling up to the Fermi level are given in Table 2. Note that these values have also been averaged over the four bonds present in equal amounts.

For comparison, an O−O COHP curve has been computed for potassium hyperoxide as a well-characterized representative compound with an anion isoelectronic to $[N_2]^{3\cdot-}$.[86] Thereby, the calculated filling is 73%, well matching the ideally expected percentage of 75% according to Scheme 1. The individual and averaged electronic character of the four N_2 entities in $Li_2Ca_3[N_2]_3$ are listed in Table 2. Accordingly, with an averaged π^* filling of 57% at zero pressure (53% at 16 GPa) resembling an expected value of 50% for diazenides, the N_2 units in $Li_2Ca_3[N_2]_3$ clearly exhibit different electronic behavior as compared to hypothetical $[N_2]^{3\cdot-}$ radical anions.

Taking these theoretical considerations into account, $Li_2Ca_3[N_2]_3$ is conjectured to consist of diazenide $[N_2]^{2-}$ ions rather than $[N_2]^{3\cdot-}$ radical anions. This assignment is probed by experiment in the next sections.

The presence of only diazenide ions in $Li_2Ca_3[N_2]_3$ and the reasonable requirement of singly (doubly) positively charged Li (Ca) ions, respectively, results in a more precise formulation as in $(Li^+)_2(Ca^{2+})_3([N_2]^{2-})_3\cdot(e^-)_2$, an anion-deficient or vice versa electron-rich structure. As prominent representatives of such compounds, suboxides or subnitrides come to mind.[87−97] Interestingly, each nitrogen atom of the diazenide entities is octahedrally coordinated by four calcium and two lithium cations. Both octahedra share one common face, which is similar to the Rb_9O_2-type cluster observed in the rubidium suboxides Rb_9O_2 and Rb_6O (see Figure 9).[87−90]

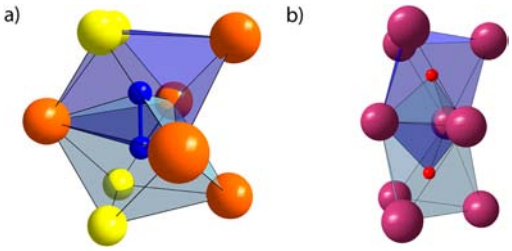

Figure 9. Coordination sphere of diazenide ions in $Li_2Ca_3[N_2]_3$ (a). Thereby each nitrogen atom is octahedrally coordinated by Li^+ and Ca^{2+}. The resulting octahedra share a common face, representing the basic motif of anion coordination in rubidium suboxides Rb_9O_2 and Rb_6O (b); Li yellow, Rb violet, Ca orange, N blue, O red.

These compounds represent oxygen-deficient (or, again, electron-rich) structures. Formally, Rb_9O_2 and Rb_6O can also be written as $(Rb^+)_9(O^{2-})_2\cdot(e^-)_5$ or $(Rb^+)_6(O^{2-})\cdot(e^-)_4$, respectively. As the $[N_2]^{2-}$ coordination spheres resemble those of the oxygen ions in suboxides and due to potential formulation of $Li_2Ca_3[N_2]_3$ as $(Li^+)_2(Ca^{2+})_3([N_2]^{2-})_3\cdot(e^-)_2$, the title compound might also constitute the first representative of hitherto unknown ternary subdiazenides. However, as compared to the Rb_9O_2 structure (see Figure 9b), with isolated Rb_9O_2 units in the rubidium-based lattice, the resulting structural motifs of N_2-coordination in $Li_2Ca_3[N_2]_3$ are exclusively interconnected again by sharing octahedral faces (see Supporting Information Figure S8).

The two independent lithium sites are coordinated by six $[N_2]^{2-}$ ions in an end-on manner, building up a strand of face-sharing octahedra (see Figures 7 and S9 in the Supporting Information). These strands are interconnected to other $^2_\infty[Li(N_2)_{6/2}]$-strands via diazenide units. The refined Li−Li distances (see Table S5 in the Supporting Information) match with reported ones.[59,98−103] Additionally, we compared the obtained Li−N distances with the sum of the ionic radii. Preliminary investigations already resulted in an average radius of one nitrogen atom in a diazenide ion to be 1.27 Å.[60] According to Shannon,[104] the ionic radius of 6-fold coordinated Li^+ is 0.76 Å. On the basis of this empirical values, the refined Li−N distances correspond well with the sum of the ionic radii.

Like hexagonal Mn_5Si_3, $Li_2Ca_3[N_2]_3$ contains structural voids, which due to the orthorhombic metric are located at (0,0,0) and (0,1/2,1/2). Many A_5B_3-type compounds were observed to incorporate nonmetal atoms like B, C, N, O, or even metals into these cavities to result in A_5B_3Z-type compounds.[82] However, a clear tendency for occupying the voids is very hard to predict. Moreover, nonstoichiometric intercalation of Z elements into the cavities is supposed to stabilize A_5B_3-type structures.[82] In $Li_2Ca_3[N_2]_3$, the average void diameter is found to be 3.15 Å (see Supporting Information Table S6), which is within the range of those in the aforementioned A_5B_3 compounds and thus formally enables incorporation of further elements into these voids. However, elemental analysis (see the Supporting Information) resulted in no significant stoichiometric atom content other than Li, Ca, and N. In addition, due to electrostatic reasons, the incorporation of cations/metals is supposed to be rather energetically unstable as shown by theoretical consideration finally resulting in $Li_2Ca_3[N_2]_3$ after removing Li atoms of Wyckoff positions 2*a* and 2*d*.

Infrared Spectroscopy. In bioinorganic chemistry, the valency of dinitrogen anions is routinely assigned according to the N−N bond lengths and their corresponding N−N stretching vibrations upon infrared or Raman spectroscopy. Recently, it has been shown experimentally that the infrared spectra of the diazenides MN_2 (M = Ca, Sr, Ba), as well as of Li_2N_2, exhibit clear features in the range of 1380−1330 cm^{-1}, which had been assigned to the N−N stretching vibration of the diazenide units.[58,59] Pernitride units as observed in noble metal $M_{NM}N_2$ compounds (M_{NM} = Os, Ir, Pd, and Pt) also exhibit distinct features around 800 cm^{-1}, attributed to the stretching of $[N_2]^{4-}$ units.[46−54] In addition, radical dinitrogen ions $[N_2]^{3\cdot-}$ have recently been observed, and they show characteristic N−N vibrations at wavenumbers shortly below 1000 cm^{-1}.[27−31]

For $Li_2Ca_3[N_2]_3$, infrared spectroscopy revealed significant features at 1260, 1100, 1020, and 802 cm^{-1} besides overtones at

dx.doi.org/10.1021/ja408816t | J. Am. Chem. Soc. 2013, 135, 16668−16679

about 3000 cm^{-1} (see Figure 10). The nitrogen dumbbells in $Li_2Ca_3[N_2]_3$ exhibit bond lengths of d_{NN} = 1.34(2)−1.35(3) Å,

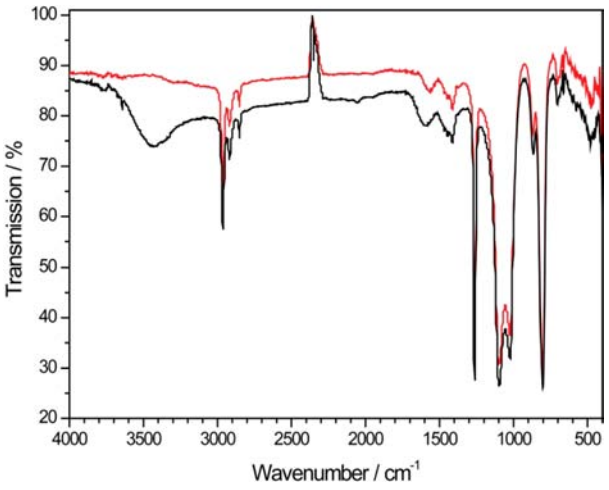

Figure 10. FTIR spectra of $Li_2Ca_3[N_2]_3$ (black) and after exposure to moisture for 5 min (red). The absorption features at about 2250 cm^{-1} are artifacts of the spectrometer.

which are intermediate to previous reports for $[N_2]^{2-}$ and $[N_2]^{3.-}$ ions. In accord with this observation, the wavenumbers of the observed features in the infrared spectrum of $Li_2Ca_3[N_2]_3$ are also intermediate to those of the latter two anions. Thus, the theoretical COHP analysis of the N−N bonding in the title compound (suggesting diazenide $[N_2]^{2-}$ ions, rather than radicals) despite elongated N−N bond lengths is in good agreement with the vibrational measurements.

Seeking again a corroboration of experimental findings, we also performed pressure-dependent phonon calculations to assign the vibrational modes from first principles, and also to look at the high-pressure trend in vibrational properties that is much more difficult to determine experimentally.

For the fully optimized (pressure-free) structural model, as well as with simulated pressures of a few GPa applied, the phonon calculations give imaginary vibrational modes (see Figure 11), which indicates dynamical instability already seen in Figure 6a (red arrow). With increasing (simulated) pressure, the imaginary modes disappear, which points toward the structure being stable under pressure.

As can further be seen in Figure 11, the theoretical phonon DOS shows a broad signal in the range from 1100 to 1300 cm^{-1} without external pressure applied, which is shifted to higher wavenumbers with increasing pressure due to shorter atomic distances. This part of the spectrum is related to the N−N stretching vibrations of the diazenide ions, and the signals are broadened because of their interaction. The experimentally obtained features at 1260, 1100, and 1020 cm^{-1} can be confirmed by the theoretical calculations, albeit caution must be taken because not all lattice modes are infrared active, and hence the IR spectrum and the computed PDOS may not be compared to each other without care.

As our calculations reveal, the feature at 800 cm^{-1} cannot be assigned to the N−N stretching vibrations of one of the diazenide units. However, the product of the high-pressure synthesis is always affected with an unknown impurity (see the Experimental Section), which might constitute an oxo- or nitridoborate originating from the BN crucible used. Such compounds exhibit distinct features at wavenumbers

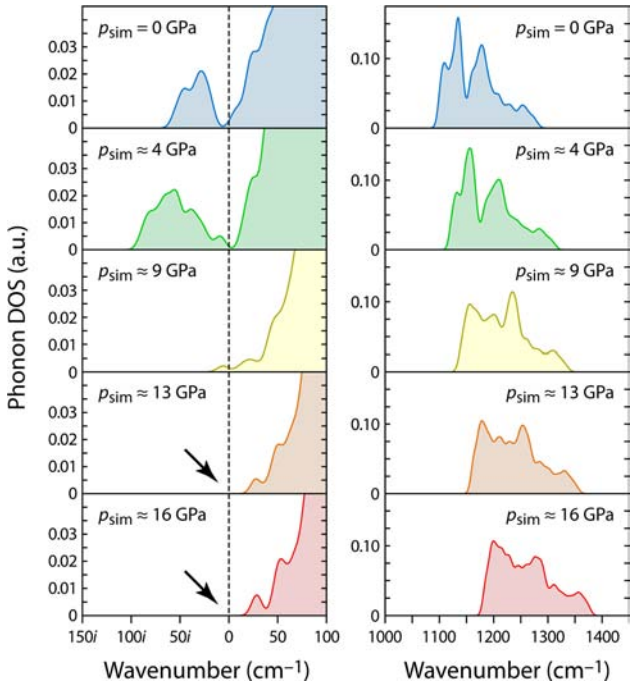

Figure 11. Excerpts from phonon densities of states computed at different simulated pressures, evolving from pressure-free structures (top) to 16 GPa. Note the absence of dynamic instabilities (that would be indicated by complex-valued vibrational modes), which sets in at increased pressure (arrows).

<1000 cm^{-1} assigned to lattice vibrations of the oxo- or nitridoborate units,[105−109] and thus might account for the unexplained signal in the IR spectrum of the title compound. A more detailed assignment of observed features in the experimental and theoretical vibrational spectrum to N−N bond lengths can be found in the Supporting Information.

Electron Spin Resonance (ESR) Spectroscopy. To settle the character of the nitrogen dumbbells experimentally, we next employed electron spin resonance spectroscopy, which is routinely used for the detection and further analysis of unpaired electrons. As the $[N_2]^{2-}$ ion is isoelectronic to molecular oxygen O_2, it should exhibit paramagnetic behavior (see Scheme 1). However, despite the paramagnetic character, the detection of an ESR-signal for molecular oxygen is hindered due to the enormous zero field splitting of the triplet state, which in general leads to a broadening and therefore makes detection of an ESR signal impossible. On the contrary, $[N_2]^{3.-}$ radical anions are shown to give a very sharp signal as they are isoelectronic to hyperoxides $[O_2]^{\cdot-}$ (see Scheme 1).[27,28] Indeed, ESR measurements of alkali and alkaline-earth hyperoxides resulted in distinct signals at a *g*-factor ranging from 2.001 to 2.004, close to the *g*-factor of free electrons (2.0023).[110,111]

Figure 12a displays the ESR spectrum of $Li_2Ca_3[N_2]_3$, whereas in Figure 12b that of BaN_2 is depicted, the latter serving as diazenide reference. The spectrum of $Li_2Ca_3[N_2]_3$ contains a narrow-line and a broad-line signal at g_{narrow} = 2.0052(1) and g_{broad} = 2.0052(10), which would, in principle, be consistent with the presence of free electrons and support a potential $[N_2]^{3.-}$ formulation. However, the ESR spectrum of BaN_2 also consists of a signal at about the *g*-factor of free electrons contradicting the unambiguous correlation of

dx.doi.org/10.1021/ja408816t | J. Am. Chem. Soc. 2013, 135, 16668−16679

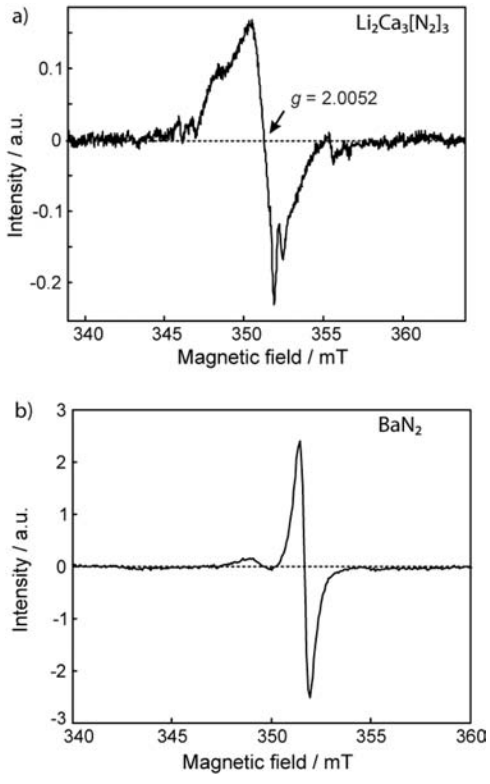

Figure 12. (a) Detail ESR spectrum at ambient temperature after background correction (black). In addition to the narrow-line signal shown here in detail, an overview spectrum (see Supporting Information Figure S3) reveals the presence of a broad-line signal. The g values for the narrow-line and the broad-line signal are 2.0052(1) and 2.0052(10), respectively. The dotted line only serves as a guide to the eyes for the zero crossing of the spectrum. (b) ESR spectrum of BaN_2 after background correction recorded at ambient temperature.

the signals in the spectrum of $Li_2Ca_3[N_2]_3$ to $[N_2]^{3-}$ radical anions.

Additionally, we analyzed the spin concentration of the obtained signals in $Li_2Ca_3[N_2]_3$ and BaN_2 and referenced them to common ESR standards. For BaN_2, the obtained spin concentration of 16.6 mM is far below the expected value of 60.8 M for the biradical $[N_2]^{2-}$. These data are in good agreement with as-mentioned difficulties in signal detection due to triplet state splitting of paramagnetic diazenide ions. Thus, the visible signal of the HP/HT product is attributed either to impurities in the mmol range or surface defects in BaN_2 evolving unpaired electrons, which then can be detected.

The ratio of double integrals of the broad-line signal of $Li_2Ca_3[N_2]_3$ to the one of the utilized one-electron references is 1:373, suggesting an effective spin concentration in $Li_2Ca_3[N_2]_3$ of 373(60) mM. The spin concentration of the narrow-line signal is only in the 10^{-3} mM range. In any case, a rough estimate indicates that the number of spins is too low for a compound with all or at least one nitrogen dumbbell in a $[N_2]^{3-}$ radical anion state. Therefore, even considering a 20% uncertainty in determining spin concentration, the observed concentration is much too low for assigning an electronic structure with $[N_2]^{3-}$ radical anions. Again, the presence of the signals is presumably due to surface defects or impurities in the sample. Taking all of these facts into account, $Li_2Ca_3[N_2]_3$ rather consists of $[N_2]^{2-}$ ions than $[N_2]^{3-}$ radical anions, which is in sound agreement with electronic-structure theory (see Figure 8).

Magnetic and Electric Conductivity Measurements. Magnetic measurements are supposed to ultimately end speculations on the potential presence of $[N_2]^{3-}$ radical anions in $Li_2Ca_3[N_2]_3$. If $Li_2Ca_3[N_2]_3$ contained $[N_2]^{3-}$ radical anions, magnetic characteristics like antiferro- or ferromagnetism would be expected as observed for the isoelectronic hyperoxides.[112] However, susceptibility measurements of $Li_2Ca_3[N_2]_3$ at 1 and 0.01 T show nearly temperature-independent (Pauli-paramagnetic) behavior down to low temperatures (see Figure 13a). To rely on this observation especially in the low-temperature region where the susceptibility slightly increases again (see Figure 13a), we also plotted the product of $\chi_{mol}T$ versus T (see Figure S11 in the Supporting Information), which resulted in a continuous increase of $\chi_{mol}T$ with increasing temperature indicative for true temperature-independent behavior of the susceptibility. This observation is in good agreement with previous magnetic measurements of again BaN_2 revealing that the dominant magnetic behavior in BaN_2 is also Pauli-paramagnetism.[39]

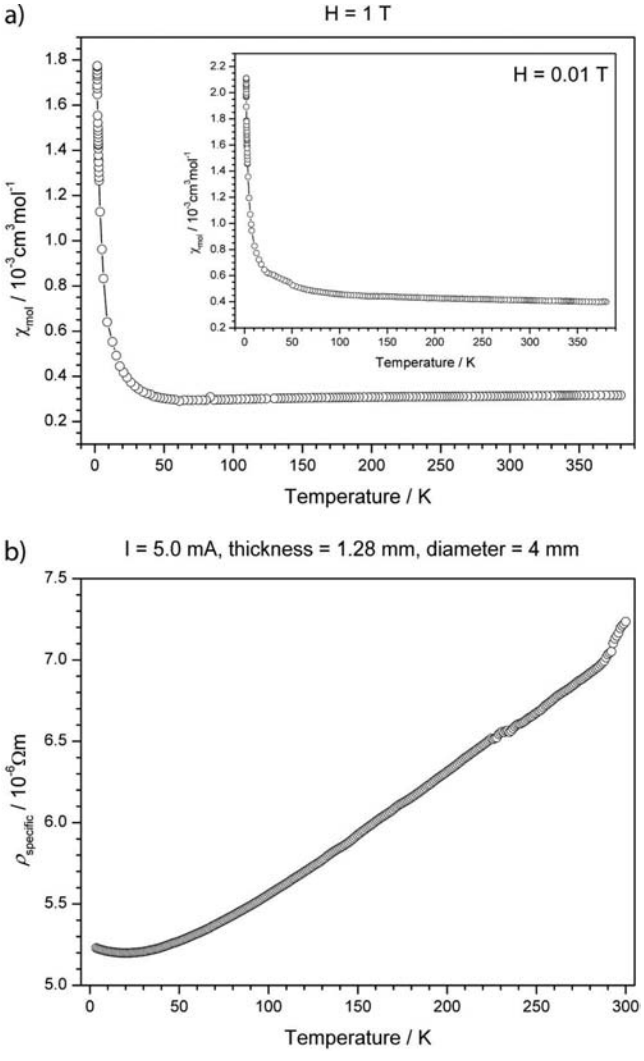

Figure 13. Course of the molar susceptibility of $Li_2Ca_3[N_2]_3$ with temperature (a) at an applied external field of 1 and 0.01 T (inset); specific resistance with temperature upon cooling (b). Error bars are not shown. The lines only serve as a guide to the eyes.

dx.doi.org/10.1021/ja408816t | J. Am. Chem. Soc. 2013, 135, 16668−16679

As shown in Figure 13b, the resistivity of $Li_2Ca_3[N_2]_3$ decreases with decreasing temperature, as is typical for metals. The resistivity at ambient temperature is found to be $7.23 \cdot 10^{-6}$ Ω m, which is in the range of good metallic conduction and qualitatively in accord with electronic-structure computations that predict a finite density of electronic states at the Fermi level (see Figure 8). Again, as-obtained results are in very good agreement with the presence of solely $[N_2]^{2-}$ ions in $Li_2Ca_3[N_2]_3$.

CONCLUSION

We were able to synthesize the first ternary compound with homonuclear dinitrogen entities by thermal decomposition of stoichiometric mixtures of ionic lithium and calcium azides under HP/HT conditions. In contrast to binary diazenides such as Li_2N_2, MN_2 (M = Ca, Sr, and Ba), and LaN_2, the ternary title compound $Li_2Ca_3[N_2]_3$ exhibits pronounced elongation of the N−N bond lengths, which would intuitively contradict the presence of $[N_2]^{2-}$ ions. In fact, these N−N distances would be better described by $[N_2]^{3\cdot-}$ units, as has been previously observed in metal-organic reference compounds.

Much to the contrary, the true character of the N_2 entity was finally elucidated by complementary use of various analytical methods. Experimental and theoretical studies excluded the presence of $[N_2]^{3\cdot-}$ radical anions, but instead supported the presence of only $[N_2]^{2-}$ ions in the crystal structure. Therefore, the ionic formulation of $Li_2Ca_3[N_2]_3$ is better described as $(Li^+)_2(Ca^{2+})_3([N_2]^{2-})_3\cdot(e^-)_2$.

Interestingly, $Li_2Ca_3[N_2]_3$ exhibits distinct structural motifs with regard to anion coordination that have been observed in Rb_9O_2- and Rb_6O-type suboxides, which represent anion-deficient (or, depending on perspective, electron-rich) structures. Within this context, the title compound might also be interpreted as the second representative of "sub-diazenides".

Finally, as compared to the classification of valencies in bound N_2 entities observed in bioinorganic or metal-organic chemistry, their adequate description in solid-state chemistry is hindered due to, for example, potential metallicity in such compounds. However, by the use of a variety of complementary methods as presented, the identification of the true oxidation state in $[N_2]^{x-}$ anions remains possible.

ASSOCIATED CONTENT

Supporting Information

Experimental details about the synthesis of azides, information about the data collection and selected crystallographic details of the Rietveld refinement of $Li_2Ca_3[N_2]_3$, analysis of temperature-dependent in situ X-ray diffraction, ESR spectroscopy, determination of the unit-cell metrics, transformation of lattice parameters and zone axes, calculation of the averaged void diameter, FTIR spectroscopy, and magnetic as well electric conductivity measurements. This material is available free of charge via the Internet at http://pubs.acs.org.

AUTHOR INFORMATION

Corresponding Author

wolfgang.schnick@uni-muenchen.de

Notes

The authors declare no competing financial interest.

ACKNOWLEDGMENTS

We would like to thank Prof. Dirk Johrendt (LMU Munich) for providing the equipment for the electric conductivity and SQUID measurements, Prof. Bettina Lotsch for providing the TEM (MPI Stuttgart), Franziska Hummel and Thomas Miller (both LMU Munich) for the low- and high-temperature powder diffraction measurements, Dr. Constantin Hoch (LMU Munich) for helpful discussions concerning the structural analysis, Nicole Dannenbauer (JMU Würzburg) for the FTIR measurements, Andreas Groß and Dr. Malte Drescher (both University Konstanz) for preliminary ESR experiments, as well as Christian Minke (LMU Munich) for solid-state MAS NMR measurements. Financial support by the Fonds der Chemischen Industrie (FCI), Deutsche Forschungsgemeinschaft (DFG), project SCHN 377/13-2, and the Max-Planck Society is gratefully acknowledged. V.L.D. is thankful to the Studienstiftung des deutschen Volkes for a scholarship.

REFERENCES

(1) Jennings, J. R. *Catalytic Ammonia Synthesis*; Plenum Press: New York, 1991.
(2) Tezcan, F. A.; Andrade, S. L. A.; Schmid, B.; Yoshida, M.; Howard, J. B.; Rees, D. C.; Einsle, O. *Science* **2002**, *297*, 1696.
(3) Burgess, B. K.; Lowe, D. J. *Chem. Rev.* **1996**, *96*, 2983.
(4) Alberty, R. A.; Goldberg, R. N. *Biochemistry* **1992**, *31*, 10610.
(5) Burgess, B. K. *Chem. Rev.* **1990**, *90*, 1377.
(6) Kim, J. S.; Rees, D. C. *Nature* **1992**, *360*, 553.
(7) Lancaster, K. M.; Roemelt, M.; Ettenhuber, P.; Hu, Y. L.; Ribbe, M. W.; Neese, F.; Bergmann, U.; DeBeer, S. *Science* **2011**, *334*, 974.
(8) Spatzal, T.; Aksoyoglu, M.; Zhang, L. M.; Andrade, S. L. A.; Schleicher, E.; Weber, S.; Rees, D. C.; Einsle, O. *Science* **2011**, *334*, 940.
(9) Thorneley, R. N. F.; Lowe, D. J. *Molybdenum Enzymes*; Wiley: New York, 1985.
(10) MacKay, B. A.; Fryzuk, M. D. *Chem. Rev.* **2004**, *104*, 385.
(11) Pickett, C. J. *J. Biol. Inorg. Chem.* **1996**, *1*, 601.
(12) Yandulov, D. V.; Schrock, R. R. *Inorg. Chem.* **2005**, *44*, 1103.
(13) Studt, F.; Tuczek, F. *J. Comput. Chem.* **2006**, *27*, 1278.
(14) Broda, H.; Hinrichsen, S.; Tuczek, F. *Coord. Chem. Rev.* **2013**, *257*, 587.
(15) Yandulov, D. V.; Schrock, R. R. *Science* **2003**, *301*, 76.
(16) Yandulov, D. V.; Schrock, R. R.; Rheingold, A. L.; Ceccarelli, C.; Davis, W. M. *Inorg. Chem.* **2003**, *42*, 796.
(17) Ritleng, V.; Yandulov, D. V.; Weare, W. W.; Schrock, R. R.; Hock, A. S.; Davis, W. M. *J. Am. Chem. Soc.* **2004**, *126*, 6150.
(18) Römer, R.; Gradert, C.; Bannwarth, A.; Peters, G.; Näther, C.; Tuczek, F. *Dalton Trans.* **2011**, 3229.
(19) Klatt, K.; Stephan, G.; Peters, G.; Tuczek, F. *Inorg. Chem.* **2008**, *47*, 6541.
(20) Stephan, G.; Peters, G.; Lehnert, N.; Habeck, C.; Näther, C.; Tuczek, F. *Can. J. Chem.* **2005**, *83*, 385.
(21) Stephan, G.; Näther, C.; Tuczek, F. *Acta Crystallogr., Sect. E* **2008**, *64*, M629.
(22) Stephan, G.; Näther, C.; Sivasankara, C.; Tuczek, F. *Inorg. Chim. Acta* **2008**, *361*, 1008.
(23) Dreher, A.; Stephan, G.; Tuczek, F. *Advances in Inorganic Chemistry. Metal Ion Controlled Reactivity*; Elsevier: Amsterdam, 2009.
(24) Pfirrmann, S.; Herwig, C.; Stößer, R.; Ziemer, B.; Limberg, C. *Angew. Chem.* **2009**, *121*, 3407; *Angew. Chem., Int. Ed.* **2009**, *48*, 3357.
(25) Smith, J. M.; Lachicotte, R. J.; Pittard, K. A.; Cundari, T. R.; Lukat-Rodgers, G.; Rodgers, K. R.; Holland, P. L. *J. Am. Chem. Soc.* **2001**, *123*, 9222.
(26) Smith, J. M.; Sadique, A. R.; Cundari, T. R.; Rodgers, K. R.; Lukat-Rodgers, G.; Lachicotte, R. J.; Flaschenriem, C. J.; Vela, J.; Holland, P. L. *J. Am. Chem. Soc.* **2006**, *128*, 756.
(27) Evans, W. J.; Fang, M.; Zucchi, G.; Furche, F.; Ziller, J. W.; Hoekstra, R. M.; Zink, J. I. *J. Am. Chem. Soc.* **2009**, *131*, 11195.

(28) Fang, M.; Bates, J. E.; Lorenz, S. E.; Lee, D. S.; Rego, D. B.; Ziller, J. W.; Furche, F.; Evans, W. J. *Inorg. Chem.* **2011**, *50*, 1459.
(29) Fang, M.; Lee, D. S.; Ziller, J. W.; Doedens, R. J.; Bates, J. E.; Furche, F.; Evans, W. J. *J. Am. Chem. Soc.* **2011**, *133*, 3784.
(30) Rinehart, J. D.; Fang, M.; Evans, W. J.; Long, J. R. *J. Am. Chem. Soc.* **2011**, *133*, 14236.
(31) Rinehart, J. D.; Fang, M.; Evans, W. J.; Long, J. R. *Nat. Chem.* **2011**, *3*, 538.
(32) Chirik, P. J. *Nat. Chem.* **2009**, *1*, 520.
(33) Kaim, W.; Sarkar, B. *Angew. Chem.* **2009**, *121*, 9573; *Angew. Chem., Int. Ed.* **2009**, *48*, 9409.
(34) Auffermann, G.; Prots, Y.; Kniep, R. *Angew. Chem.* **2001**, *113*, 565; *Angew. Chem., Int. Ed.* **2001**, *40*, 547.
(35) Auffermann, G.; Prots, Y.; Kniep, R.; Parker, S. F.; Bennington, S. M. *ChemPhysChem* **2002**, *9*, 815.
(36) Auffermann, G.; Schmidt, U.; Bayer, B.; Prots, Y.; Kniep, R. *Anal. Bioanal. Chem.* **2002**, *373*, 880.
(37) Auffermann, G.; Kniep, R.; Bronger, W. *Z. Anorg. Allg. Chem.* **2006**, *632*, 565.
(38) Prots, Y.; Auffermann, G.; Tovar, M.; Kniep, R. *Angew. Chem.* **2002**, *114*, 2392; *Angew. Chem, Int. Ed.* **2002**, *41*, 2288.
(39) Vajenine, G. V.; Auffermann, G.; Prots, Y.; Schelle, W.; Kremer, R. K.; Simon, A.; Kniep, R. *Inorg. Chem.* **2001**, *40*, 4866.
(40) Holleman, A. F.; Wiberg, E. *Lehrbuch der Anorganischen Chemie*; de Gruyter: Berlin/New York, 2007.
(41) Wiberg, N.; Fischer, G.; Bachhuber, H. *Chem. Ber.* **1974**, *107*, 1456.
(42) Bondybey, V. E.; Nibler, J. W. *J. Chem. Phys.* **1973**, *58*, 2125.
(43) Blau, E. J.; Hochheimer, B. F. *J. Chem. Phys.* **1964**, *41*, 1174.
(44) Rosengren, K.; Pimentel, G. C. *J. Chem. Phys.* **1965**, *43*, 507.
(45) Minkwitz, R. *Z. Anorg. Allg. Chem.* **1975**, *411*, 1.
(46) Gregoryanz, E.; Sanloup, C.; Somayazulu, M.; Badro, J.; Fiquet, G.; Mao, H.-K.; Hemely, R. J. *Nat. Mater.* **2004**, *3*, 294.
(47) von Appen, J.; Lumey, M.-W.; Dronskowski, R. *Angew. Chem.* **2006**, *118*, 4472; *Angew. Chem., Int. Ed.* **2006**, *45*, 4365.
(48) Crowhurst, J. C.; Goncharov, A. F.; Sadigh, B.; Evans, C. L.; Morrall, P. G.; Ferreira, J. L.; Nelson, A. J. *Science* **2006**, *311*, 1275.
(49) Young, A. F.; Montoya, J. A.; Sanloup, C.; Lazzeri, M.; Gregoryanz, E.; Scandolo, S. *Phys. Rev. B* **2006**, *73*, 153102.
(50) Montoya, J. A.; Hernandez, A. D.; Sanloup, C.; Gregoryanz, E.; Scandolo, S. *Appl. Phys. Lett.* **2007**, *90*, 011909.
(51) Crowhurst, J. C.; Goncharov, A. F.; Sadigh, B.; Zaug, J. M.; Aberg, D.; Meng, Y.; Prakapenka, V. B. *J. Mater. Res.* **2008**, *23*, 1.
(52) Chen, Z. W.; Guo, X. J.; Liu, Z. Y.; Ma, M. Z.; Jing, Q.; Li, G.; Zhang, X. Y.; Li, L. X.; Wang, Q.; Tian, Y. J.; Liu, R. P. *Phys. Rev. B* **2007**, *75*, 054103.
(53) Yu, R.; Zhan, Q.; De Jonghe, L. C. *Angew. Chem.* **2007**, *119*, 1154; *Angew. Chem., Int. Ed.* **2007**, *46*, 1136.
(54) Wessel, M.; Dronskowski, R. *J. Am. Chem. Soc.* **2010**, *132*, 2421.
(55) Allen, N. T.; Kennard, O.; Watson, D. G.; Brammer, L.; Orpen, A. G.; Taylor, R. *J. Chem. Soc., Perkin Trans.* **1987**, *2*, S1.
(56) Sutton, L. E. *Tables of Interatomic Distances and Configuration in Molecules and Ions*; Chemical Society Spec. Publ. 11, Chemical Society: London, 1958.
(57) Giguère, P. A.; Liu, I. D. *J. Chem. Phys.* **1952**, *20*, 136.
(58) Schneider, S. B.; Frankovsky, R.; Schnick, W. *Inorg. Chem.* **2012**, *51*, 2366.
(59) Schneider, S. B.; Frankovsky, R.; Schnick, W. *Angew. Chem.* **2012**, *124*, 1909; *Angew. Chem., Int. Ed.* **2012**, *51*, 1873.
(60) Wessel, M.; Dronskowski, R. *J. Comput. Chem.* **2010**, *31*, 1613.
(61) Zhang, X.; Zunger, A.; Trimarchi, G. *J. Chem. Phys.* **2010**, *133*, 194504.
(62) Tschauner, O.; Luo, S. N.; Chen, Y. J.; McDowell, A.; Knight, J.; Clark, S. M. *High Pressure Res.* **2013**, *33*, 202.
(63) Walker, D.; Carpenter, M. A.; Hitch, C. M. *Am. Mineral.* **1990**, *75*, 1020.
(64) Walker, D. *Am. Mineral.* **1991**, *76*, 1092.
(65) Huppertz, H. *Z. Kristallogr.* **2004**, *219*, 330.
(66) Rubie, D. C. *Phase Transitions* **1999**, *68*, 431.
(67) Kawai, N.; Endo, S. *Rev. Sci. Instrum.* **1970**, *8*, 1178.
(68) Coelho, A. A. *TOPAS-Academic, Version 4.1*; Coelho Software: Brisbane, 2007.
(69) Bergmann, J.; Kleeberg, R.; Haase, A.; Breidenstein, B. *Mater. Sci. Forum* **2000**, *303*, 347.
(70) Spek, A. L. *PLATON, A Multipurpose Crystallographic Tool, v1.07*; Utrecht University: Netherlands, 2003.
(71) Stadelmann, P. A. *Ultramicroscopy* **1987**, *21*, 131.
(72) Perdew, J. P.; Burke, K.; Ernzerhof, M. *Phys. Rev. Lett.* **1996**, *77*, 3865−3868.
(73) Blöchl, P. E. *Phys. Rev. B* **1994**, *50*, 17953.
(74) (a) Kresse, G.; Hafner, J. *Phys. Rev. B* **1993**, *47*, 558. (b) Kresse, G.; Furthmüller, J. *Comput. Mater. Sci.* **1996**, *6*, 15. (c) Kresse, G.; Furthmüller, J. *Phys. Rev. B* **1996**, *54*, 11169. (d) Kresse, G.; Joubert, D. *Phys. Rev. B* **1999**, *59*, 1758.
(75) Monkhorst, H. J.; Pack, J. D. *Phys. Rev. B* **1976**, *13*, 5188.
(76) Dronskowski, R.; Blöchl, P. E. *J. Phys. Chem.* **1993**, *97*, 8617.
(77) (a) Andersen, O. K. *Phys. Rev. B* **1975**, *12*, 3060. (b) Andersen, O. K.; Jepsen, O. *Phys. Rev. Lett.* **1984**, *83*, 2571.
(78) von Barth, U.; Hedin, L. *J. Phys. C: Solid State Phys.* **1972**, *5*, 1629.
(79) Parlinski, K.; Li, Z. Q.; Kawazoe, Y. *Phys. Rev. Lett.* **1997**, *78*, 4063.
(80) Togo, A.; Oba, F.; Tanaka, I. *Phys. Rev. B* **2008**, *78*, 134106.
(81) Stoffel, R. P.; Dronskowski, R. *Z. Anorg. Allg. Chem.* **2013**, *639*, 1227.
(82) Corbett, J. D.; Carcia, E.; Guloy, A. M.; Hurng, W.-M.; Kwon, Y.-U.; Leon-Escamilla, E. A. *Chem. Mater.* **1998**, *10*, 2824.
(83) Aronsson, B. *Acta Chem. Scand.* **1960**, *14*, 1414.
(84) Schachner, H.; Cerwenka, E.; Nowotny, H. *Monatsh. Chem.* **1954**, *85*, 241.
(85) Kulkarni, A.; Schön, J. C.; Doll, K.; Jansen, M. *Chem.-Asian J.* **2013**, *8*, 743.
(86) The structure was taken from an earlier experimental report in: Smith, H. G.; Nicklow, R. M.; Raubenheimer, L. J.; Wilkinson, M. K. *J. Appl. Phys.* **1966**, *37*, 1047 with d(O−O) = 1.25 Å. Test computations including full relaxation at the GGA level were also performed, giving a quite different d(O−O) = 1.34 Å. Nonetheless, COHPs computed for the analogous optimized structure lead to a π^* occupation of 74%, which is within 1% of that given in Figure 8 (right) for the experimental structure. We conclude that the relative filling of the π^* orbital does not seem strongly affected by the structural optimization.
(87) Simon, A. *Z. Anorg. Allg. Chem.* **1977**, *431*, 5.
(88) Simon, A.; Deiseroth, H. J. *Rev. Chim. Miner.* **1976**, *13*, 98.
(89) Simon, A. *Molecular Clusters of the Main Group Elements*; Wiley-VCH: Weinheim, 2004.
(90) Simon, A. *Crystal Structure and Chemical Bonding in Inorganic Chemistry*; North-Holland Publ. Comb.: Amsterdam, 1975.
(91) Simon, A. *Z. Anorg. Allg. Chem.* **1973**, *395*, 301.
(92) Simon, A. *Z. Anorg. Allg. Chem.* **1977**, *428*, 187.
(93) Tsai, K.-R.; Harris, P.; Lassettre, E. *J. Phys. Chem.* **1956**, *60*, 338.
(94) Simon, A. *Struct. Bonding (Berlin)* **1979**, *36*, 81.
(95) Rauch, P.; Simon, A. *Angew. Chem.* **1992**, *104*, 1505; *Angew. Chem., Int. Ed.* **1992**, *31*, 1519.
(96) Snyder, G.; Simon, A. *J. Am. Chem. Soc.* **1995**, *117*, 1996.
(97) Snyder, G.; Simon, A. *Angew. Chem.* **1994**, *106*, 713; *Angew. Chem., Int. Ed.* **1994**, *33*, 689.
(98) Rabenau, A.; Schulz, H. *J. Less-Common Met.* **1976**, *50*, 155.
(99) Cota, L. G.; De La Mora, P. *Acta Crystallogr., Sect. B* **2005**, *61*, 133.
(100) Fischer, D.; Jansen, M. *Z. Anorg. Chem.* **2003**, *629*, 1934.
(101) Hellner, E.; Laves, F. *Z. Kristallogr.* **1943**, *105*, 134.
(102) Reckeweg, O.; Simon, A. *Z. Naturforsch., B* **2003**, *85*, 1097.
(103) (a) Zintl, E.; Brauer, G. *Z. Elektrochemistry* **1935**, *41*, 102. (b) Rabenau, A.; Schultz, H. *J. Less-Common Met.* **1976**, *50*, 155. (c) Brese, N. E.; O'Keeffe, M. *Structural Bonding*; Springer: Berlin, 1992.
(104) Shannon, R. D. *Acta Crystallogr., Sect. A* **1976**, *32*, 751.

(105) Ren, M.; Lin, J. H.; Dong, Y.; Yang, L. Q.; Su, M. Z.; You, L. P. *Chem. Mater.* **1999**, *11*, 1576.
(106) Laperches, J. P.; Tarte, P. *Spectrochim. Acta* **1966**, *22*, 1201.
(107) Blasse, G.; van den Heuvel, G. P. M. *Phys. Status Solidi* **1973**, *19*, 111.
(108) Somer, M. *Z. Naturforsch.* **1991**, *46b*, 1664.
(109) Kaindl, R.; Sohr, G.; Huppertz, H. *Spectrochim. Acta, Part A* **2013**, *116*, 408.
(110) Khan, A. U.; Mahanti, S. D. *J. Chem. Phys.* **1975**, *63*, 2271.
(111) Belevskii, V. N.; Vol'nov, I. I.; Tokareva, S. A. *Bull. Acad. Sci. USSR* **1972**, *21*, 1366.
(112) Zumsteg, A.; Ziegler, M.; Känzig, W.; Bösch, M. *Phys. Condens. Matter* **1974**, *17*, 267.